COMMUNICATION

MRI of NSCs on Carbon Scaffolds

ADVANCED
HEALTHCARE
MATERIALS

www.advhealthmat.de

3D Carbon Scaffolds for Neural Stem Cell Culture and Magnetic Resonance Imaging

Erwin Fuhrer, Anne Bäcker, Stephanie Kraft, Friederike J. Gruhl, Matthias Kirsch, Neil MacKinnon, Jan G. Korvink, and Swati Sharma*

3D glassy carbon structures with percolated macropores are obtained by pyrolysis of chemically synthesized cryogels featuring tunable porosity. These batch-fabricated structures are used as scaffolds for culturing neural stem cells (NSCs) and are characterized by magnetic resonance imaging (MRI). With the aid of MRI, the successful cultivation of NSCs on a glassy carbon surface and the precise 3D locations of these cell clusters within the opaque scaffold are demonstrated. MRI also yields pore morphology and porosity analyses, pre- and post-pyrolysis. This integrated approach yields a complete 3D dataset of the NSC network, which enables the visual inspection of the morphological details of individual cell clusters without disturbing them or destroying the scaffold. Reported experimental methodology is expected to have an impact on studies designed to understand the mechanism of neurodegenerative disease (ND) development, and can serve as a protocol for the culture of various other types of cells that display compatibility with glassy carbon surfaces.

In vitro cell culture systems are valuable experimental systems for studying topics ranging from fundamental molecular biology to understanding disease initiation, progression, and potential treatment options.[1] They relieve the dependence on animal studies; however, only in cases where the culture system reliably replicates the in vivo context can the culture results be trusted alternatives of the relevant animal model experiments. A significant challenge that must be addressed is the dimensionality of the culture system. Many in vitro assays are 2D substrate systems, which raises the question of the relevance to tissues that thrive in a 3D environment. Since it has been recognized that the scaffold topology imparts important cues for cell development and function, there has been a concerted effort to develop 3D scaffold systems that better reproduce the in vivo environment.

Common materials used for 3D scaffold fabrication for various cell differentiation, angiogenesis, and tumor growth studies include commercially available Matrigel, hydrogels, and cryogels.[2] Matrigel is a gelatinous protein mixture that contains components of the basement membrane, such as laminin, collagen type IV, and entactin.[3] Hydrogels (water-containing polymer networks) are composed of either natural polymers such as collagen, hyaluronates, fibrin, and chitosan or synthetic polymers such as polyvinyl caprolactam and polyethylene glycol.[4] These materials are generally advantageous since a 3D hydrated network can be produced together with the desired chemical cues required for cell development (e.g., growth factors and cell adhesion promoters). In addition, the porous structure (size and shape) of the polymer network can be tuned by varying the freezing conditions and concentration of the cross-linker in the case of cryogels.[5,6] However, several disadvantages can be identified. Matrigel is often poorly chemically defined and thus culture-to-culture variation has been observed.[7] Hydrogels may require further chemical processing to introduce the important cellular chemical cues.[8] This introduces the potential for residual chemicals to be entrapped within the gel, influencing the reproducibility of cell development. These materials additionally have the potential to degrade after prolonged exposure to culture media. While not always an issue, in cases of extended culture times, cell cultures require a scaffold that will maintain its mechanical integrity. In this work, we propose glassy carbon as a material capable of overcoming these challenges.

Conversion of polymer structures into glassy carbon using pyrolysis is a widespread process that is extensively used for the fabrication of carbon MEMS and NEMS,[9,10] battery and supercapacitor anodes,[11] and carbon nanofibers.[12,13] One very attractive yet rather unexplored feature of glassy carbon is its excellent cytocompatibility,[14–18] which, in combination with its mechanical strength,[9] inertness, and patternability,[10] makes it a very suitable material for the fabrication of 3D cell culture platforms.

E. Fuhrer, Dr. A. Bäcker, Dr. F. J. Gruhl, Dr. N. MacKinnon,
Prof. J. G. Korvink, Dr. S. Sharma
Institute of Microstructure Technology
Karlsruhe Institute of Technology
Hermann-von-Helmholtz-Platz 1
76344 Eggenstein-Leopoldshafen, Germany
E-mail: swati.sharma@kit.edu
Dr. S. Kraft, Dr. M. Kirsch
Institute of Anatomy and Cell Biology
Department of Neuroanatomy
Faculty of Medicine
University of Freiburg
Albertstrasse 23, 79104 Freiburg, Germany

The ORCID identification number(s) for the author(s) of this article can be found under https://doi.org/10.1002/adhm.201700915.

A few research groups have reported on using glassy carbon substrates for cell culture, but have mainly employed lithographically patterned 2D or 2.5D structures adhered on to a silicon surface,[14,16,17] or bulk carbon nanofiber webs as scaffolds.[19,20] While these structures do substantiate glassy carbon's suitability for in vitro biological studies, they have yet to utilize its full potential in terms of fabrication of tailor-made porous scaffolds.

Glassy carbon is also a well-known electrode material[16,21,22] suitable for providing an electrical stimulus to the cells and observing their response. It has been demonstrated that glassy carbon surface can support neurite growth under electric field-mediated culture conditions,[16] which validates its cytocompatibility in an electrochemical environment. Additionally, it is generally free of any impurities or contamination (the high-temperature process renders its surface sterile and inert) that may lead to corrosion or cause an undesired physical environment for the cells. Interestingly, while various microfabricated patterns involving complicated techniques are being investigated for obtaining glassy carbon scaffolds, the straightforward pyrolysis of porous hydrogels, which are often readily available to biologists, has gone completely unnoticed.

Besides scaffold material selection, there remains a general challenge to be addressed in all 3D cell culture systems. Observation of cellular development and activity is most often an optical measurement. Thus, a cellular network existing within the pores of a 3D polymer network is difficult to observe noninvasively and nondestructively. While carbon can address many of the 3D scaffold challenges, the fact that it is virtually nontransparent highlights the requirement for a nonperturbing measurement methodology.

Magnetic resonance imaging (MRI) is capable of meeting this challenge as it is already a widespread imaging technique in medicine that has found applications in cell and tissue imaging.[23,24] The technique holds tremendous potential as a noninvasive cell characterization tool that allows the extraction of 3D cellular network data. A very attractive feature of MRI is the range of applicable acquisition sequences that facilitate the control of the obtained image contrast. These contrast mechanisms, based on local ^1H relaxation differences, enable a clear identification of both the cellular network and the scaffold structure. MR microscopy of *Aplysia* neurons,[24] transplanted neural stem cells (NSCs),[25] and alpha motor neurons[23] in animal tissue slices has been reported with spatial resolution down to 3 µm. Spectroscopic measurements (NMR) have been performed on cell suspensions[26] and scaffold cultures (e.g., hollow fiber membranes).[27] However, to our knowledge, there has not been a report of MRI measurements being performed on cultured cells.

The multidisciplinary experimental approach used in this work is illustrated in **Figure 1**. To demonstrate the proposed cell culture and measurement protocol, NSCs cultured on pyrolyzed cryogels were chosen since (i) NSCs have already been reported to show an affinity to the pyrolytic carbon surface[15–17] and (ii) studies that rely on understanding the collective behavior of cells in a 3D cellular microenvironment, for example, those aimed at understanding the mechanism of neurodegenerative disease (ND) development, can benefit the most from our noninvasive imaging technique. Moreover, since ND studies require a long-term cell culture (often 6–8 weeks), carbon's mechanical strength, chemical inertness, and resistance to swelling are advantageous. It must be noted that the cell culture and imaging method reported here is not limited to NSCs, and we believe most cell types can be adapted to this versatile technique.

An important feature of 3D scaffolds is the porosity. It is well known that pyrolysis will cause isotropic shrinkage of the
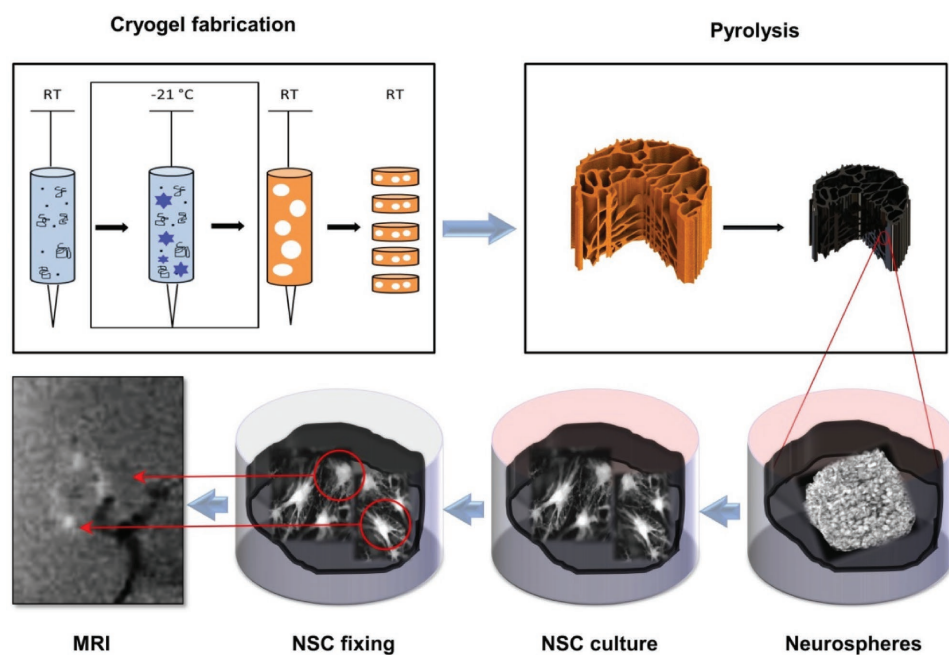
Figure 1. Process flow showing cryogel synthesis, pyrolysis, NSC culture, fixing, and MRI. This protocol could be generalized to any carbonizable precursor polymer and carbon-compatible cell type.
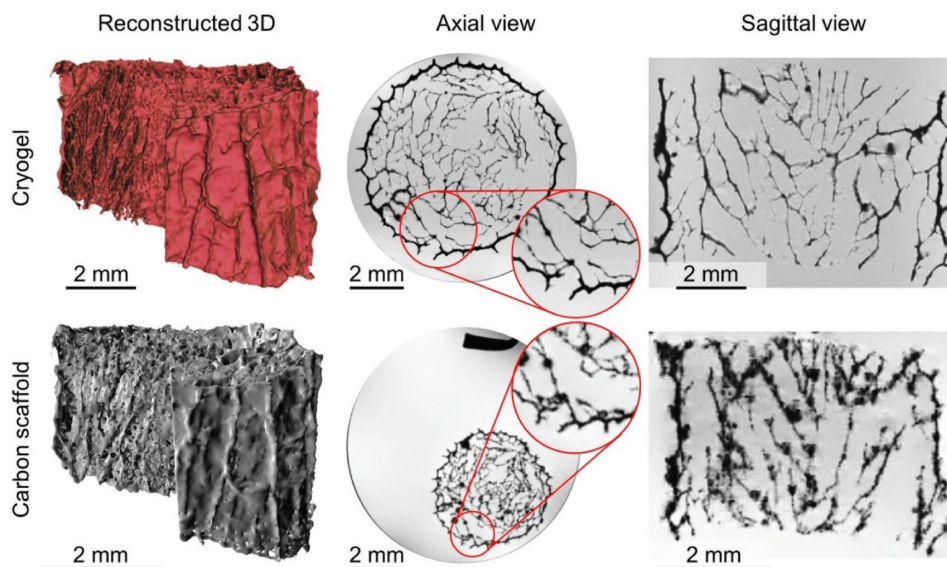
Figure 2. Porosity analysis and 3D modeling using MRI dataset. Left column: 3D reconstruction with identical perspectives of the same structure before (top) and after (bottom) pyrolysis, including a cropped corner to expose interior view. Middle column: MR images of axial slices. Insets highlight retained morphology with size reduction. Right column: sagittal slices with same perspectives of cryogel and carbon scaffold. The pore network is observed to be highly interconnected, including vertical channels through the entire structure.

precursor structure,[12] and therefore porosity must be evaluated pre- and post-pyrolysis. In addition to being well suited to biomaterial imaging, MRI is a natural choice to comparatively image a cryogel and its resulting carbon scaffold. Other commonly used porosity measurement methods are unsuitable for a direct structural comparison due to technical limitations. For example, mercury intrusion porosimetry (MIP) is destructive,[28,29] while nitrogen adsorption isotherms[30] are measured at 77 K, resulting in a perturbed cryogel structure. MRI also reveals the degree of heterogeneity in the porous network and yields a dataset that can be postprocessed employing advanced processing tools such as 3D Slicer to obtain 3D visuals of the porous structures (see the Experimental Section). For this purpose, samples were prepared by immersing the scaffold in $CuSO_4$-doped H_2O within a vacuum chamber to reduce trapped air bubbles (see the Supporting Information for sample preparation details). All MR images for porosity analysis were obtained with 30 µm isotropic resolution using a 3D gradient echo (GRE) sequence. After taking into consideration the various contributions to voxel intensity, and processing intensity thresholds (see the Supporting Information for a detailed discussion), MR images and representative reconstructed 3D models of a cryogel and its pyrolyzed counterpart were obtained as displayed in **Figure 2**. Typical porosity and surface-to-volume ratio values extracted from 3D reconstructed models are 83% ± 4% and 6.8 ± 0.5 and 58% ± 6% and 11.5 ± 0.5 before and after carbonization of cryogels, respectively. To extract the binary dataset from the original data, automatic thresholding method suggested by Otsu was used.[31]

As has been observed for various carbonizable polymers, the pyrolysis protocol did not change the overall morphology of the structure, except for isotropic shrinkage (volume change on carbonization: 221 ± 9 to 48 ± 2 mm³).[10,12] Evidently, the overall porosity decreases, while the surface-to-volume ratio almost doubles upon carbonization, suggesting a more densely packed structure, which was confirmed by scanning electron microscopy (SEM) (**Figure 3**A,B). Of notable importance is the heterogeneity of the pore structures, which in general are elongated cylinders in the direction parallel to the main gel axis, highlighting the degree of approximation in the MIP analyses.

NSCs have been successfully cultured on glassy carbon,[15–17,19] and these observations were replicated in this work using the carbon 3D scaffolds. After obtaining the initial evidence from SEM and fluorescence microscopy (shown in Figure 3C and D–F, respectively), MR images of fixed NSCs cultured on carbon scaffolds were acquired. Scaffolds were directly imaged in the phosphate buffer used for fixing but without $CuSO_4$ (a contrast agent). Notably, the scaffold was physically broken in order to facilitate the SEM and optical observations of cell clusters residing within the porous structure while MRI was conducted nondestructively.

In **Figure 4**, various MR images and movies (Supporting Information) are presented. MR imaging was performed by running a T_1-weighted 3D GRE sequence in which we observed greater signal intensity from NSC clusters compared to buffer solution. Hence, NSC clusters can be identified as bright regions, while the scaffold material appears dark. In Figure 4A–H, an optical image followed by a series of MR images (subsequent slices) of an NSC cluster can be observed. The 3D data obtained from the entire scaffold structure can be further processed to reveal the NSC network with specific locations of the cells.

By segmentation into dark and bright voxels, two datasets were created: the dark voxels for the carbon structure and bright voxels for cell clusters. Superposition of the two and subsequent 3D visualization allows one to display and examine the cell distribution inside the carbon scaffold as demonstrated in Figure 4I,J (screenshots from movie files in the Supporting
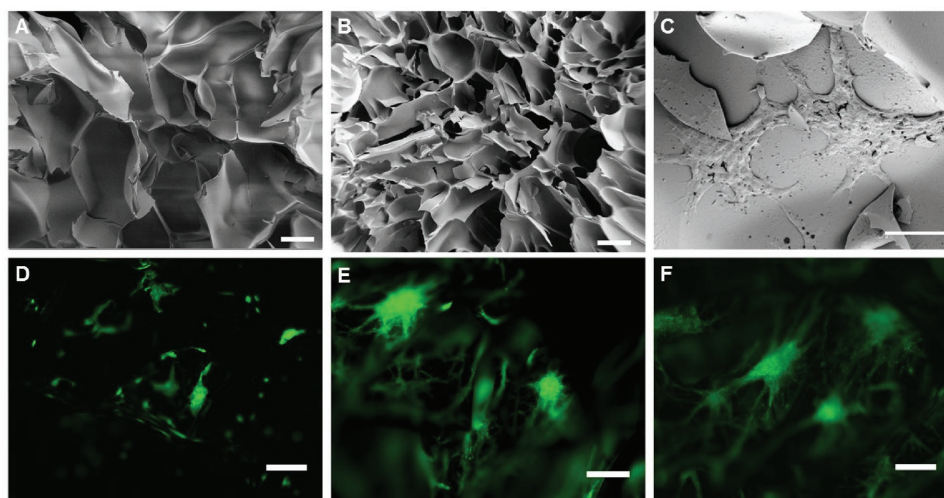
Figure 3. Scanning electron microscopy images and fluorescence microscopy images (scale bar: 200 µm in all cases). SEM images of cryogel A) before and B) after pyrolysis, and C) cultured NSCs on carbon scaffold surface; D–F) fluorescence microscopy images of NSCs on carbon surface at 10× magnification.

Information). Finally, a reconstructed 3D model of a small section of NSC containing scaffold is shown in Figure 4K.

Although reported MR images are obtained for fixed NSCs, a preliminary test was conducted on active cells in order to evaluate if they survive through the MRI sessions within the carbon scaffolds. For this purpose, cells extracted from a broken scaffold that had been subjected to two consecutive overnight MRI runs were reseeded. Optical images of neurospheres regrown from the dissociated cells (provided in the Supporting Information) indicate that NSCs can be successfully recultured from

the neurospheres post-MRI. This experiment further substantiates a viable NSC culture on 3D glassy carbon scaffolds.

An additional benefit of using MR-based imaging is the possibility to measure NMR spectra of the system. NMR spectroscopy reveals the chemical composition of the sample, and could be used to monitor major metabolites as a method to assess the health of the culture (e.g., sufficient nutrient supply, excess waste buildup, and stress response). As a proof of concept, NMR spectra for a model chemical mixture in the presence of the scaffolds are presented in the Supporting Information.
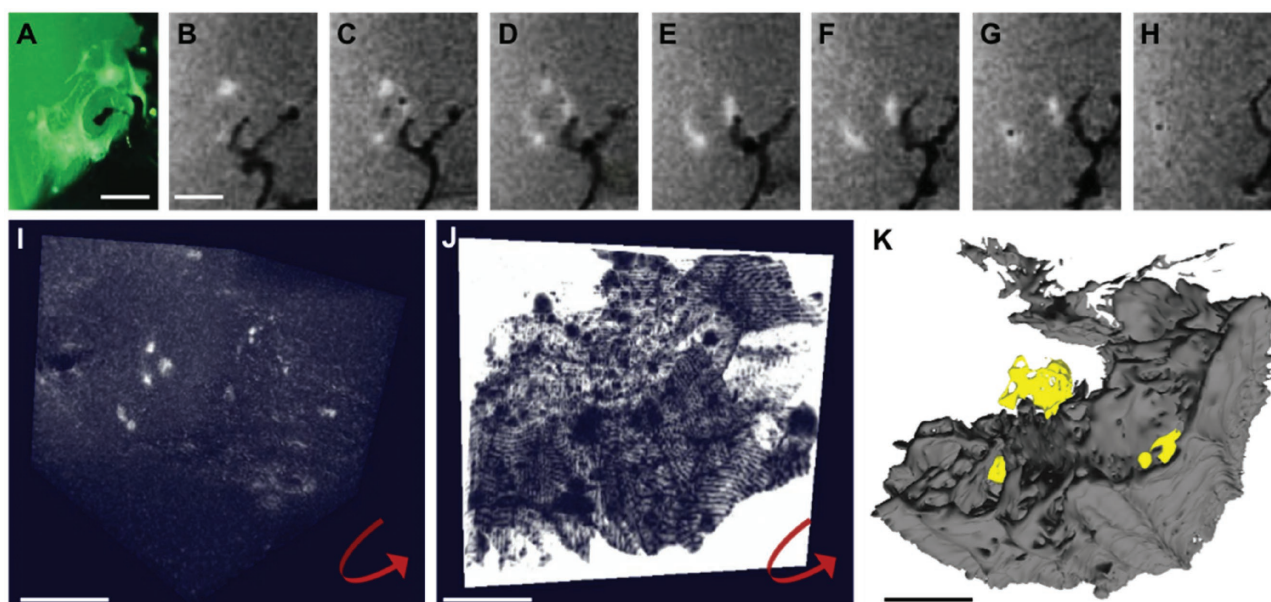
Figure 4. MRI of NSCs cultured on a glassy carbon scaffold. A) An optical image of the NSC cluster; B–H) corresponding MR images showing NSC clusters in a series of sagittal slices [scale bar: 400 µm, shown in panels (A) and (B)]. 3D extraction of I) cellular network and J) carbon scaffold (screenshots; video files in the Supporting Information). K) 3D model of a subsection of scaffold containing NSCs. Yellow regions indicate cell clusters [scale bar: 1 mm in panels (I)–(K)].

We also characterized the scaffolds using cyclic voltammetry (CV) in order to evaluate their suitability for neural electrodes. Featureless cyclic voltammograms (see the Supporting Information) suggest a capacitive behavior with the linear electrode capacitance of ≈ 24 µF. This supports the hypothesis that cryogel-derived carbon exhibits similar electrochemical stability and inertness as glassy carbon derived from other polymers.[16]

In summary, we have demonstrated a multidisciplinary experimental scheme by combining four diverse research fields: cryogel synthesis, carbonization, NSC culture, and MRI. This protocol can potentially be adapted to address a range of biological questions. All postculture experiments are performed at room temperature and can in principle be performed on active culture systems with the aid of MR-compatible bioreactors that would enable detailed cell viability studies as a future development. Reported measurements were performed on fixed cells in order to first develop a protocol with optimized fabrication and MRI parameters. MRI serves as an efficient, noninvasive, and nondestructive imaging tool with a large field of view (FOV) (see the Experimental Section and Supporting Information for details) that facilitates monitoring of a cell population and the network formation behavior. Thus, we propose this integrated approach for gaining insight into the mechanism of ND development, progression, and treatment response, which is currently only possible using animal models. The alternative 2D cell culture systems are useful for understanding the basic molecular relationships but are far removed from modeling the complex microenvironment of the central nervous system. ND studies can also benefit from simultaneous spectroscopic observation to validate the imaging data and to predict cellular responses.

MRI-assisted porosity analysis has broader applications, including in studies in which hydrogels are used as scaffold materials. Most porosity measurement techniques are only capable of analyzing materials in the dry state. Hydrogel morphology is strongly dependent on the hydration level, and thus such measurements would not reflect the porosity of the scaffold when immersed in culture media. MRI is a natural alternative to determine porosity in such systems, under the condition that the pore sizes are larger than the MR image resolution (on the order of tens of micrometers). Current MRI limitations include signal-to-noise ratio and contrast-to-noise ratio (SNR and CNR) requirements for an improved identification of cell-containing voxels. Here one can explore diffusion weighted imaging (DWI), various suppression techniques, or the addition of medically approved contrast agents for selective highlighting of desired target tissues. Further enhancement of SNR can be achieved by the application of MR microcoils that yield resolution down to 3 µm or provide much faster scanning times.[23] This would entail microfabricated scaffolds, tailored to suit the geometric requirements of the microcoil.

Pyrolysis of polymers is expected to result in a completely new approach for scaffold fabrication methods, since a number of carbonizable polymers are compatible with micro- and nanofabrication. As a result, structures generated by advanced fabrication technologies (e.g., two-photon lithography) can be pyrolyzed[32] to produce cell culture scaffolds featuring microcoil-compatible custom geometry. Their conversion to carbon will preserve the topology while removing any undesired substances (such as residual monomers or photoinitiators) that may be toxic for cells over longer periods of culture. By taking advantage of material shrinkage, custom scaffolds in the direction of single cell analyses could be produced. In addition to complex geometries, the fact that glassy carbon is electrically conductive has yet to be explored as an additional degree of freedom in cell culture studies. Such functionality could be used for both stimulation and sensing (e.g., for dopamine production).

Experimental Section

Cryogel Synthesis: Cryogels were prepared using the protocol developed by Kumar and Srivastava[33] using 1% chitosan, 6% agarose, and 2% gelatin in the initial aqueous mixture.

Pyrolysis: Pyrolysis was performed in a tube furnace (Heraeus GmbH) in inert environment at 900 °C (ramp rate: 3 °C min^{-1}; dwell time at 900 °C: 1 h) followed by natural cooling to room temperature.[10]

NSC Culture: Neurosphere cultures were prepared from the subventricular zone (SVZ) of adult male mice (6–8 weeks of age) and grown for 5 d in growth medium composed of Neurobasal A, B27 (2%), GlutaMax (2×10^{-3} M), L-glutamine (1×10^{-3} M), penicillin/streptomycin (both at 100 µg mL^{-1}), recombinant murine epidermal growth factor (EGF; 20 ng mL^{-1}), and recombinant human basic fibroblast growth factor (bFGF; 10 ng mL^{-1}). All media and supplements were procured from Life Technologies/Thermo Fisher Scientific (Darmstadt, Germany), and growth factors were from PeproTech (Hamburg, Germany). Carbon scaffolds were sterilized by immersion in isopropanol, washed with water, and equilibrated with growth medium overnight. Prior to seeding cells, scaffolds were placed in growth medium in an exicator for 2–3 h at room temperature to remove air from the pores. For seeding the neurospheres on the scaffold, they were dissociated with Accutase and 250 000 cells in 5 µL of growth medium were seeded on top of the carbon scaffolds followed by incubation at 37 °C in 5% CO$_2$ for 30 min to allow the cells to settle. Subsequently, the carbon scaffolds were carefully transferred to the growth medium in individual wells of a 48-well plate and cultured for 4 d, with a 50% medium change after 2 d in culture. Cultured cells were then fixed with paraformaldehyde in phosphate buffer for evaluation of formed NSC structures with the aid of SEM (Supra 60VP, Zeiss), fluorescence imaging (DM5500B, Leica), and MRI (500 MHz NMR System, Bruker BioSpin).

For post-MRI cell reculture, the scaffolds were kept in 1.5 mL medium in an Eppendorf tube for a total of 40 h in a culture medium similar to the one mentioned above, with the exception that Neurobasal A was replaced by a CO$_2$-independent medium, Hibernate A. After performing MRI, the scaffolds were crushed carefully and a single cell suspension, inevitably containing fragments of the scaffold, was obtained by incubation for 10 min at 37 °C in Accutase. Cells were then reseeded in regular culture medium and cultured for 5 d to allow for the formation of spheres.

MRI: All MR experiments were performed on a Bruker Avance III Wide-Bore NMR system with Micro-5 probe operating at ^{1}H frequency of 500 MHz. 5 and 10 mm saddle coils (5 and 10 mm) were used for NSC measurements and porosity analysis, respectively. For porosity analysis, cryogel and carbon scaffolds were immersed in CuSO$_4$ solution of 12 mg L^{-1}, which yielded relaxation times of $T_1 = 24$ ms and $T_2 = 17$ ms. MR acquisition parameters were: 3D GRE, echo time (TE) = 7 ms, repetition time (TR) = 50 ms, flip angle (FA) = 80°, receiving bandwidth (BW) = 22.5 kHz, and the number of acquisitions (NEX) = 46, leading to a total scan time of 65 h 25 min 20 s with an isotropic resolution of 30 µm. The matrix size for cryogel analysis was $230 \times 320 \times 320$ and for carbon scaffold analysis $160 \times 320 \times 320$. The samples were transferred into the NMR tube under vacuum ($\approx$1 mbar). Cultured NSCs were imaged directly in the buffer solution used for fixing (without contrast agent or additional vacuum treatment) using these parameters: 3D GRE, TE = 2.75 ms, TR = 100 ms, FA = 45°, BW = 100 kHz, and NEX = 19,

leading to a total scan time of 13 h 30 min 40 s. The matrix size was $160 \times 160 \times 320$ with an isotropic resolution of 31.25 μm.

CV: Cyclic voltammetric measurements were performed using an EG&G 273A potentiostat (Princeton Applied Research) in 0.1 M phosphate-buffered saline (pH 7.4) in the specific potential range −0.3 to +0.6 V in a three-electrode system consisting of a suspended carbon scaffold (without cells) as the working electrode, graphite rod as the counter electrode, and saturated calomel as the reference electrode. The scaffold was characterized at two potential scan rates, 50 and 100 mV s^{-1}. Linear capacitance was determined using Equation (1), where C represents the capacitance, i is the measured current, and du/dt is the voltage scan rate. Further details can be found in the Supporting Information

$$C = \frac{i}{du/dt} \qquad (1)$$

Porosity Analysis: The MRI data were exported as DICOM files from ParaVision 6.0 (Bruker BioSpin). For thresholding, the data were imported to MATLAB and binarized by applying the built-in function greythres, which uses Otsu's method based on discriminant analysis.[31] The binarized image was saved as DICOM file and imported to the software 3D Slicer. Based on the binarized dataset, the 3D models were generated using the built-in function ModelMaker. Volume and surface data of the scaffolds were extracted from the 3D models.

Supporting Information

Supporting Information is available from the Wiley Online Library or from the author.

Acknowledgements

Conflict of Interest

The authors declare no conflict of interest.

Keywords

[1] M. Ravi, V. Paramesh, S. Kaviya, E. Anuradha, F. P. Solomon, *J. Cell. Physiol.* **2015**, *230*, 16.
[2] E. Knight, S. Przyborski, *J. Anat.* **2015**, *227*, 746.
[3] H. K. Kleinman, G. R. Martin, *Semin. Cancer Biol.* **2005**, *15*, 378.
[4] M. W. Tibbitt, K. S. Anseth, *Biotechnol. Bioeng.* **2009**, *103*, 655.
[5] X. Zhao, J. Kim, C. A. Cezar, N. Huebsch, K. Lee, K. Bouhadir, D. J. Mooney, *Proc. Natl. Acad. Sci. USA* **2011**, *108*, 67.
[6] S. Bhat, A. Tripathi, A. Kumar, *J. R. Soc. Interface* **2011**, *8*, 540.
[7] M. C. Cushing, K. S. Anseth, *Science* **2007**, *316*, 1133.
[8] I. M. El-Sherbiny, M. H. Yacoub, *Glob. Cardiol. Sci. Pract.* **2013**.
[9] O. J. A. Schueller, S. T. Brittain, C. Marzolin, G. M. Whitesides, *Chem. Mater.* **1997**, *9*, 1399.
[10] S. Sharma, M. Madou, *Bioinspired Biomimetic Nanobiomater.* **2012**, *1*, 252.
[11] S. Sharma, R. Kamath, M. Madou, *J. Anal. Appl. Pyrolysis* **2014**, *108*, 12.
[12] G. M. Jenkins, *Polymeric Carbons—Carbon Fibre, Glass and Char*, Cambridge University Press, Cambridge **1976**.
[13] W. Zhang, *J. Med. Biol. Eng.* **2014**, *34*, 386.
[14] G. T. Teixidor, R. A. Gorkin, III, P. P. Tripathi, G. S. Bisht, M. Kulkarni, T. K. Maiti, T. K. Battacharyya, J. R. Subramaniam, A. Sharma, B. Y. Park, M. Madou, *Biomed. Mater.* **2008**, *3*, 034116.
[15] J. Mitra, S. Jain, A. Sharma, B. Basu, *Carbon* **2013**, *65*, 140.
[16] S. Jain, A. Sharma, B. Basu, *Biomaterials* **2013**, *34*, 9252.
[17] L. Amato, A. Heiskanen, C. Caviglia, F. Shah, K. Zór, M. Skolimowski, M. Madou, L. Gammelgaard, R. Hansen, E. G. Seiz, M. Ramos, T. Moreno Ramos, A. Martínez-Serrano, S. S. Keller, J. Emnéus, *Adv. Funct. Mater.* **2014**, *24*, 7042.
[18] V. Pesáková, Z. Klézl, K. Balík, M. Adam, *J. Mater. Sci.: Mater. Med.* **2000**, *11*, 793.
[19] S. Jain, A. Sharma, B. Basu, *J. Biomed. Mater. Res., Part B: Appl. Biomater.* **2013**, *101B*, 520.
[20] S. Jain, T. J. Webster, A. Sharma, B. Basu, *Biomaterials* **2013**, *34*, 4891.
[21] B. Uslu, S. A. Ozkan, *Anal. Lett.* **2007**, *40*, 817.
[22] M. Vomero, E. Castagnola, F. Ciarpella, E. Maggiolini, N. Goshi, E. Zucchini, S. Carli, L. Fadiga, S. Kassegne, D. Ricci, *Sci. Rep.* **2017**, *7*, 40332.
[23] J. J. Flint, C. H. Lee, B. Hansen, M. Fey, D. Schmidig, J. D. Bui, M. A. King, P. Vestergaard-Poulsen, S. J. Blackband, *NeuroImage* **2009**, *46*, 1037.
[24] G. Radecki, R. Nargeot, I. O. Jelescu, D. Le Bihan, L. Ciobanu, *Proc. Natl. Acad. Sci. USA* **2014**, *111*, 8667.
[25] S. M. C. Berman, P. Walczak, J. W. Bulte, in *Magnetic Resonance Neuroimaging: Methods and Protocols*, Vol. *711* (Eds: E. Modo, J. W. M. Bolte), Humana Press, Totowa, NJ **2011**.
[26] K. R. Foster, J. L. Schepps, R. D. Stoy, H. P. Schwan, *Phys. Med. Biol.* **1979**, *24*, 1177.
[27] M. Augath, P. Heiler, S. Kirsch, L. R. Schad, *J. Magn. Reson.* **2009**, *200*, 134.
[28] N. Kathuria, A. Tripathi, K. K. Kar, A. Kumar, *Acta Biomater.* **2009**, *5*, 406.
[29] A. Abell, K. Willis, D. Lange, *J. Colloid Interface Sci.* **1999**, *211*, 39.
[30] K. Sing, *Colloids Surf. A: Physicochem. Eng. Aspects* **2001**, *187–188*, 3.
[31] N. Otsu, *IEEE Trans. Syst. Man Cybern.* **1979**, *9*, 62.
[32] A. Zakhurdaeva, P.-I. Dietrich, H. Hölscher, C. Koos, J. G. Korvink, S. Sharma, *Micromachines* **2017**, *8*, 285.
[33] A. Kumar, A. Srivastava, *Nat. Protoc.* **2010**, *5*, 1737.